Supplement to "Measurements of spectral irradiance during the solar eclipse of 21 August 2017: reassessment of the effect of solar limb darkening and of changes in total ozone"

Germar Bernhard[1], Boyan Petkov[2]

[1]Biospherical Instruments Inc., San Diego, CA 92110, USA
[2]Institute of Atmospheric Sciences and Climate (ISAC) of the Italian National Research Council (CNR), I-40129 Bologna, Italy

Correspondence to: Germar Bernhard (bernhard@biospherical.com)

S1 Calibration of GUVis-3511 data measured during the solar eclipse of 21 August 2017

In this sections, subscripts *S* and *L* refer to "Sun" and "Lamp" respectively. The objective of the calibration is to determine the spectral solar irradiance $\overline{E}_S(\lambda)$ at the instrument's collector, referenced to a spectral resolution of 1 nm. More specifically, $\overline{E}_S(\lambda)$ is defined via

$$\overline{E}_S(\lambda) = \frac{\int E_S(\lambda')s(\lambda-\lambda')d\lambda'}{\int s(\lambda')d\lambda'}, \quad \text{(S1)}$$

where λ and λ' are wavelengths, $s(\lambda)$ is a triangular function with a bandwidth of 1 nm full width at half maximum (FWHM), and $E_S(\lambda)$ is the solar spectrum (either global or partly shaded by the BioSHADE) at its native spectral resolution. The numerator of Eq. (S1) is the solar spectrum convolved with function $s(\lambda)$ and the denominator is a normalization term. When measurements of the GUVis-3511 are calibrated according to this definition, they would be identical to measurements of a hypothetical spectroradiometer with slit function $s(\lambda)$. Note also that $E(\lambda)$ and $\overline{E}(\lambda)$ can differ by more than a factor of 10 because of the Fraunhofer structure in the solar spectrum, which can vary greatly within a 1 nm bandpass at certain wavelength ranges in the UV (see for example Fig. 2 by Bernhard et al. (1999)).

S1.1 Lamp based calibration

All channels with the exception of the two 305 nm channels and the 313 nm channel were calibrated using a 1000-W FEL tungsten lamp. The spectral irradiance from this lamp at a distance of 50 cm is traceable to the scale of spectral irradiance established by the U.S. National Institute of Standards and Technology in 2000 (Yoon et al., 2000).

The calibration of the instrument is based on the principle that the "net" signal V_i reported by channel i of a multi-filter instrument is proportional to the spectral irradiance $E(\lambda)$ weighted with this channel's response functions $r_i(\lambda)$ (Seckmeyer et al., 2010):

$$V_i = \gamma_i \times \int E(\lambda) r_i(\lambda) d\lambda \,, \tag{S2}$$

where γ_i is a proportionality constant and $\hat{E}(\lambda_i) \equiv \int E(\lambda) r_i(\lambda) d\lambda$ is called the "response-weighted irradiance" of channel i. The net signal V_i is the difference between the "light" signal measured with the unoccluded irradiance collector and the "dark" signal measured with the collector covered with an opaque cap.

By evaluating Eq. (S2) separately for the spectrum of the calibration lamp, $E_L(\lambda)$, and a solar spectrum measured during the solar eclipse, $E_S(\lambda)$, and combining the results, we obtain:

$$\int E_S(\lambda) r_i(\lambda) d\lambda = \frac{V_{S,i}}{V_{L,i}} \int E_L(\lambda) r_i(\lambda) d\lambda \,, \tag{S3}$$

where $V_{S,i}$ is the net signal of channel i when measuring solar radiation and $V_{L,i}$ is the net signal when the instrument's collector is facing the calibration lamp. Note that all terms on the right side of Eq. (S3) are known. The term on the left side is the response-weighted solar irradiance $\hat{E}_S(\lambda_i) \equiv \int E_S(\lambda) r_i(\lambda) d\lambda$ and includes the unknown term $E_S(\lambda)$.

In the last step of the calibration routine, the solar spectral irradiance as defined by Eq. (S1) and evaluated at the nominal wavelength λ_i of channel i, $\overline{E}_S(\lambda_i)$, is calculated from $\hat{E}_S(\lambda_i)$ with the help of radiative transfer calculations:

$$\overline{E}_S(\lambda_i) \approx \hat{E}_S(\lambda_i)\frac{\int E_S^*(\lambda)s_i(\lambda)d\lambda}{\int E_S^*(\lambda)r_i(\lambda)d\lambda} = \hat{E}_S(\lambda_i)\times C_i\,, \tag{S4}$$

where $E_S^*(\lambda)$ is the solar spectral irradiance calculated with a radiative transfer model and C_i is a conversion factor defined by Eq. (S4). This conversion factor converts the response-weighted solar irradiance $\hat{E}_S(\lambda_i)$ to the solar spectral irradiance $\overline{E}_S(\lambda_i)$. Note that Eq. (S4) is not exact (hence the symbol "≈") because the modeled solar spectrum $E_S^*(\lambda)$ may differ from the true solar spectrum $E_S(\lambda)$. Note also that any wavelength-independent differences between $E_S^*(\lambda)$ and $E_S(\lambda)$ do not result in systematic errors. Such errors become only significant if differences between the two quantities change greatly over the wavelength range where $r_i(\lambda)$ is different from zero. This is typically only the case in ranges where atmospheric gases have large, wavelength-dependent absorption features, such as the absorption by ozone in the UV-B, and water vapor in the infrared.

S1.1.1 Calculation of conversion factors C_i

All measurements during the eclipse were converted with a single model spectra $E_S^*(\lambda)$, which was calculated with the libRadtran/UVSPEC radiative transfer (RT) model version 1.01 (Mayer and Kylling, 2005). Calculations of global spectral irradiance were performed with the sdisort RT solver using 12 streams. The solar zenith angle (SZA) was set to 33.55°, which corresponds to a time of 19:00:30 shortly after the end of the eclipse. For wavelength below 630 nm, the extraterrestrial solar spectrum used for modeling was the spectrum $E_{Gueymard}(\lambda)$ defined in Eq. (2) of Bernhard et al. (2004). The spectrum is available at http://uv.biospherical.com/Version2/Paper/2004JD004937-ETS_GUEYMARD.txt. Above 630 nm, the spectrum described by Gueymard (2004) was used. Profiles of atmospheric pressure, temperature, and trace gases were taken from the Air Force Geophysics Laboratory (AFGL) atmospheric constituent profile for mid-latitude summer (Anderson et al., 1986). The ozone profile was scaled to a total ozone column (TOC) of 298 DU in accordance with measurements by the Ozone Monitoring Instrument (OMI) on the Aura satellite (Sect. 7.4). Ozone absorption cross section data measured by Bass and Paur (1985) were used. The surface albedo was set to 0.05. Aerosol extinction was parameterized with Ångström's turbidity formula by setting the Ångström coefficients α and β to 2.1 and 0.0394, respectively. These values were derived from the instrument's measurement of direct solar irradiance (Sect. 7.3). The aerosol single scattering albedo was set to 0.95 and the aerosol asymmetry parameter to 0.7. The precipitable water column was set 22 kg/m^2. Results shown in Sect. 7.1 indicate that this was a reasonable value for the period of measurements. Attenuation by water vapor was

modeled with the correlated-k method of the LOWTRAN/SBDART model (Ricchiazzi et al., 1998), which is part of libRadtran. Associated uncertainties will be discussed in Sect. S1.3.

S1.1.2 Sensitivity analysis of conversion factor

A sensitivity analysis was performed to quantify the dependence of $\overline{E}_S(\lambda_i)$ on the choice of model parameters. Specifically, the factor C_i for converting $\hat{E}_S(\lambda_i)$ to $\overline{E}_S(\lambda_i)$ was re-calculated with the following settings: (Case 1) SZA = 61° (corresponding to SZA at 16:04 shortly before the start of eclipse); (Case 2) SZA = 48° and modeling for diffuse instead of global irradiance (to simulate solar spectrum during the time of totality); (Case 3) TOC = 305 DU (to estimate the uncertainty in the conversion resulting from the uncertainty in TOC); and (Case 4) TOC = 254 DU (to simulate the effect of low ozone that was observed during the vicarious calibration of the 305 and 313 nm channels discussed in Sect. S1.2). Uncertainties in the conversion according to Eq. (S4) depend not only on the model spectrum but also on uncertainties in the measurements of the spectral response functions $r_i(\lambda)$. These functions were not only measured at BSI (Fig. 3) but also by the Norwegian Radiation Protection Authority (NRPA). Values of $\overline{E}_S(\lambda_i)$ calculated with the two sets of characterization data were also compared (Case 5).

Results of the sensitivity analysis are shown in Fig. S1. For channels with wavelengths between 320 and 875 nm, plus the 1,020 nm channel, conversion factors calculated with the five parameterizations differ by less than ±1% from the reference. Channels at 305 and 313 nm are affected by changes in ozone, but maximum difference remain below about ±2%. The conversion factor for the 940 nm channel depends greatly on the SZA due to water vapor absorption at this wavelength. However, this is of little importance for studying solar limb darkening (Sect. 7.1) because the relevant data are normalized to model calculations (e.g., Fig. 8c) and the effect on SZA is for the most part removed when discussing solar limb darkening effects at this wavelength. Still, absolute values of the spectral irradiance at 940 nm are subject to a large uncertainty.

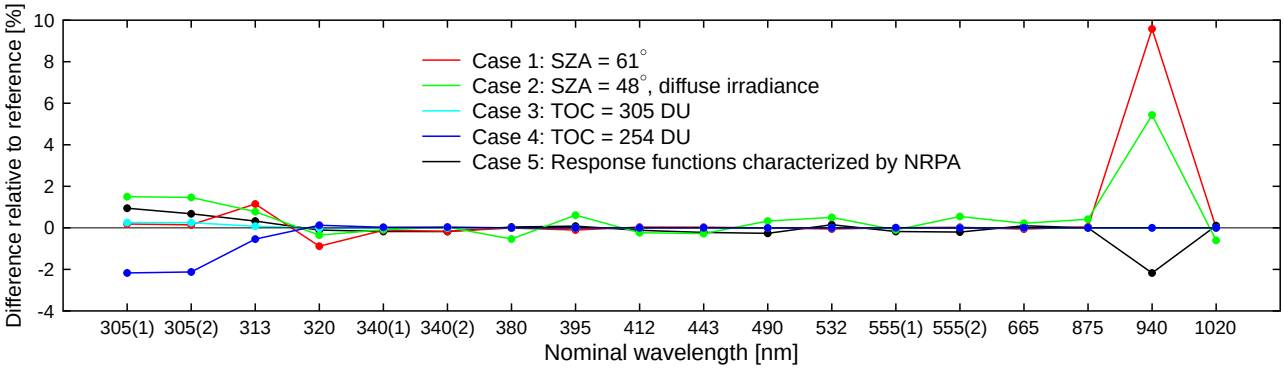

Fig. S1. Comparison of conversation factors C_i, calculated with various model parameters relative to the reference set of model parameters. Wavelengths measured by more than one channel are indicated by (1) and (2) on the x-axis.

S1.2 Vicarious calibration

Calibrating the 305 and 313 nm channels with the method describes above is subject to comparatively large uncertainties because of the large change of the solar spectrum in the UV-B range and the mismatch between solar and lamp spectra in this wavelength range. For example, the spectral response functions of both 305 channels are different from zero between 272 and 313 nm, and all wavelengths within this range contribute to the signal $V_{L,i}$ when measuring the calibration lamp. In contrast, spectral solar irradiances below 290 nm are virtually zero and do not contribute to $V_{S,i}$. Because of this mismatch, small errors in the wavelength mapping of spectral response functions $r_i(\lambda)$ can lead to large errors in the conversion factor (Seckmeyer et al., 2010). To reduce calibration uncertainties of the two 305 channels and the 313 nm channel, their measurements were vicariously calibrated against a SUV-100 spectroradiometer located in San Diego, which is part of the National Science Foundation's Ultraviolet Spectral Irradiance Monitoring Network (UVSIMN) (Booth et al., 1994). The GUVis-3511 was set up next to the SUV-100 instrument between 22 and 25 November 2017, a period with no clouds and minimal aerosol loading. SUV-100 data were converted to "Version 2" data products (Bernhard et al., 2004), which have a spectral resolution of 1 nm, are referenced to the same triangular function that was used in Eq. (S1), and are corrected for the cosine response error of the spectroradiometer. Calibration factors K_i for the GUVis-3511 where calculated by regressing GUV net signals $V_{S,i}$ against spectral irradiances $\overline{E}_{S,SUV}(\lambda)$ measured the SUV-100. Spectral irradiances of the GUV, $\overline{E}_{S,GUV}(\lambda_i)$, were finally obtained by applying these calibration factors to $V_{S,i}$:

$$\overline{E}_{S,GUV}(\lambda_i) = \frac{V_{S,i}}{K_i}. \quad \text{(S5)}$$

When plotting $\overline{E}_{S,GUV}(\lambda_i)$ versus $\overline{E}_{S,SUV}(\lambda)$, data points are generally not located on a straight line because the solar spectrum in the UV-B shifts to longer wavelengths as the SZA increases. This problem was mitigated by calibrating GUV measurements against SUV measurements using SUV data at *different* wavelengths than those indicate by the GUV's nominal wavelengths. This method is illustrated in Fig. S2, which shows ratios of $\overline{E}_{S,GUV}(\lambda_i) / \overline{E}_{S,SUV}(\lambda)$ plotted versus SZA for different wavelengths λ used in $\overline{E}_{S,SUV}(\lambda)$. When GUV measurements of the two 305 nm channels are calibrated against SUV measurements at 305 nm, GUV/SUV ratios are too large for SZAs larger than 60°. In contrast, ratios are too small, when calibrating against the spectral irradiance at 307 nm. Ratios obtained by calibrating against the spectral irradiance at 306 nm are almost constant for SZA smaller than 65°, suggesting that 306 nm is close to the optimum wavelength.

The smallest SZA during the calibration period in late November 2017 was 53° and data from this period do not allow to assess the relationship between GUV and SUV data for smaller SZAs. However, similar calibrations of the radiometer in early September 2014 (where the minimum SZA was 25°) indicated that this ratio varies by less than ±3% for SZA between 25 and 70° (orange symbols in Fig. S2a), suggesting that the maximum uncertainty of GUV data for the SZA range of relevance to the eclipse measurements is 3%. (Note that the 2014 calibration cannot be used for the calibration of eclipse data because the instrument's collector was modified between 2014 and 2017, which changed the channels' sensitivities.)

A similar analysis was also performed for the 313 nm channel and it was determined that calibrations against SUV measurements at 315 resulted in the least dependence of the GUV/SUV ratio on SZA (Fig. S2b). Based on these results, GUV measurements of the 305 and 313 nm channels were vicariously calibrated against spectral irradiance from the SUV-100 using measurements at 306 and 315 nm, respectively, and data from the two channels reported in Sect. 7 therefore refer to 306 and 315 nm.

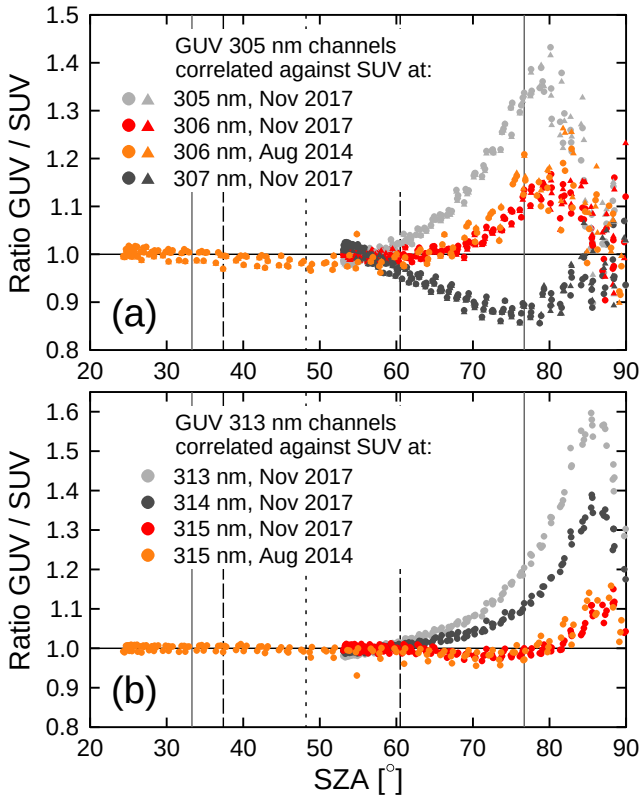

Fig. S2. Ratio of spectral irradiances measured by the GUVis-3511 and SUV-100 radiometers at San Diego. (a) Ratios of calibrated GUV measurements of the two 305 nm channels against spectral irradiance measured by the SUV-100 at 305, 306 and 307 nm. Circles and triangles refer to the GUV's 1st and 2nd 305 nm channel, respectively. (b) Ratio of calibrated GUV measurements of the 313 nm channels against spectral irradiance measured by the SUV-100 at 313, 314 and 315 nm. Vertical grey lines indicate the SZA range when measurements on 21 August 2017 were performed. Long-dashed lines indicate the SZA range of the eclipse and the short-dashed line indicates the SZA at the time of totality.

S1.3 Uncertainty budget

The uncertainty of spectral irradiance measurements during the solar eclipse was calculated from the following components: the uncertainty of the scale of spectral irradiance issued by NIST; the uncertainty of transferring the scale of spectral irradiance from a NIST standard to a working standard; the uncertainty in measuring the net signals of the GUVis-3511 facing the working standard; the uncertainty in characterizing the spectral response functions $r_i(\lambda)$; uncertainties resulting from changes in the dark current during solar measurements; drift of the sensitivity of the GUV's channels between calibration and deployment, uncertainties of the cosine-error correction; and uncertainties caused by non-linearity.

The irradiance scale of BSI's calibration lamps and that of the SUV-100 spectroradiometer are traceable to the NIST standard F-616, which was calibrated by NIST on 11 August 2008 and had less than six hours of runtime. The expanded ($k = 2$) uncertainty according to the lamp's NIST certificate is 1.74 % at 250 nm, 1.27 % at 350, and less than 1 % between 450 and 1,600 nm. The voltage drop across the lamp's terminals when operating at the nominal current of 8.2 A agrees to within 0.01 V (0.01%) with the voltage measured by NIST, indicating that the lamp output has not changed during transport

from NIST to BSI. The standard (k = 1) uncertainty of the transfer of the irradiance scale of lamp F-616 to the working standard that was used to calibrate the GUVis-3511 is estimated to 0.2 %. The uncertainty in measuring the net signal of the GUVis-3511 radiometer facing the working standard is 0.55 % and was calculated from uncertainties of the lamp current, radiometer-to-lamp distance, lamp alignment, stray light in the calibration laboratory, instrument noise and potential drift of the working standards' calibration since its calibration against the lamp F-616.

The propagation of errors in the measurement of the spectral response functions $r_i(\lambda)$ to measurements of $\hat{E}_S(\lambda_i)$ is a multi-dimensional problem and difficult to quantify. We therefore estimate this uncertainty component from the difference of $\hat{E}_S(\lambda_i)$ derived from either using our measurement of $r_i(\lambda)$ or those performed at NRPA (black line in Fig. S1). The so-derived standard uncertainty for channels with wavelength between 320 and 875 nm is 0.2 %. The uncertainty in the conversion factors C_i arising from changes in SZA and other atmospheric parameters is 0.2 % and was also estimated from the data presented in Fig. S1.

The instrument's dark current was measured three times during the duration of the eclipse by covering the collector with an opaque cap. These measurements did not indicate a drift in the dark current and related uncertainties were therefore set to zero. The drift of the sensitivity of the GUV's channels between calibration and deployment was estimated from a comparison of lamp calibration performed on 30 August 2017 and 5 February 2018. The responsivities calculated from data collected at the calibration events agreed to within ±1.3 % for channels with wavelengths smaller than 340 nm and to within ±0.4 % for the remaining channels.

Cosine-error correction factors varied between 0.944 and 1.026 over the period of measurements and between 0.978 and 1.020 for the period of the eclipse. Standard uncertainties were set to 0.5 %, which is one quarter of this range. Lastly, uncertainties caused by a non-linearity were not determined, however, results shown in Sect. 7.1 do not indicate any non-linearity (see al Sect. 8.4).

As explained in Sect. S1.2, the calibration of the 305 and 313 nm channel is based on a vicarious calibration against version 2 data of the SUV-100 spectroradiometer. The expanded (k = 2) uncertainty of version 2 data from a SUV-100 radiometer identical to the one used in San Diego is 6.4% at 310 nm (or 3.2% for k = 1) according to Bernhard et al. (2004),

and this uncertainty is also used here. The uncertainty of transferring the calibration from the SUV-100 to the GUVis-3511 is 1 % and was estimated from data presented in Fig. S2.

The total ozone column during the calibration at San Diego was 254 DU while it was 298 DU during the solar eclipse. Conversation factors shown in Fig. S1 for the two ozone columns differ by 2% for the 305 nm channels and we therefore assume an additional uncertainty of 1 % (k = 1) for the vicarious calibration. Uncertainties related to dark current drifts, change in sensitivity, cosine-error correction, and non-linearity are identical for the lamp and vicarious calibrations.

The uncertainty budget for all channels but the 940 nm channel is provided in Table S1. Expanded uncertainties for the 305 and 313 nm channels range between 7.3 and 7.5% and are dominated by the uncertainty of SUV measurements. Expanded uncertainties of the other channels are 2.7 %. An uncertainty budget for the 940 nm channel is not provided here because of the large effect of the SZA on conversion factor C_i of this channel (Fig. S1). Measurements of this channel should therefore be used with caution. However, when the SZA is corrected using a radiative transfer model (Sect. 7.1), variations in measurements of this channel during the solar eclipse due to solar limb darkening agree well with measurements of the adjacent channels at 875 and 1,020 nm.

Even though published solar irradiances for the 305 and 313 nm channels are based on the vicarious calibration and measurements at 320 and 340 nm on the lamp-based calibration, we calibrated the four channels with both approaches and compared the results. Measurements of the 305 nm channels calibrated with the methods differ by 18 % and we attribute this large difference to the large uncertainty in establishing a lamp-based calibration for this channel. Difference in solar irradiances calculated with the two method for the 313, 320 and 340 channels are 1.1 %, 0.7 %, and 4.1 %, and are within the combined uncertainties of the two methods.

Table S1. Uncertainty budget of GUVis-3511 measurements.

	Relative Standard Uncertainty, %		
Error source	305 nm	313 nm	320 - 1,020 nm
NIST standard			1.0
lamp transfer			0.2
Measurement net signal			0.6
Response function			0.2
SUV-100 uncertainty	3.2	3.2	
Transfer SUV-100 to GUVis-3511	1	1	
Dark current	0.0	0.0	0.0
Sensitivity drift	1.3	1.3	0.4
Conversion factor	1.0	0.3	0.2
Cosine-error correction	0.5	0.5	0.5
Combined uncertainty	3.8	3.6	1.4
Expanded uncertainty (*k* = 2)	**7.5**	**7.3**	**2.7**

Wavelengths 305 and 313 nm refer to nominal wavelengths.

S2 Calculating total ozone column from 305 / 313 and 313/ 340 wavelength pairs

In Sect. 7.4., calculations of TOC from the 305 / 340 wavelength pair were presented and discussed. Figure S3 shows similar results calculated from the wavelengths pairs 305 / 313 and 313 / 340. These TOCs were calculated using look-up tables as described in Sect. 5.2.

Fig. S3a shows results without limb darkening (LD) correction. TOCs for the 305 / 340 pair (blue) are identical with the "uncorrected" data shown in Fig. 13. Ozone values for the 313 / 340 pair are *smaller* than those of the 305 / 340 pair and exhibit a negative slope as a function of time. In contrast, ozone values for the 305 / 313 pair are *larger* than those of the 305 / 340 pair and exhibit a positive slope. These biases are likely caused by a small systematic error in measurements of the 313 nm channel. When measurements of this channels are scaled with a factor of 0.95 and ozone retrievals repeated, TOCs derived from the three wavelengths pairs are consistent to within ±2.5 DU outside the period of the eclipse (Fig. S3b). A systematic error of 5 % is well within the expanded uncertainty of 7.3% of the 313 nm channel (see Table S1). Using this adjustment, measurements of all pairs also agree to within 5 DU (1.7 %) with OMI data (red line in Figure S3).

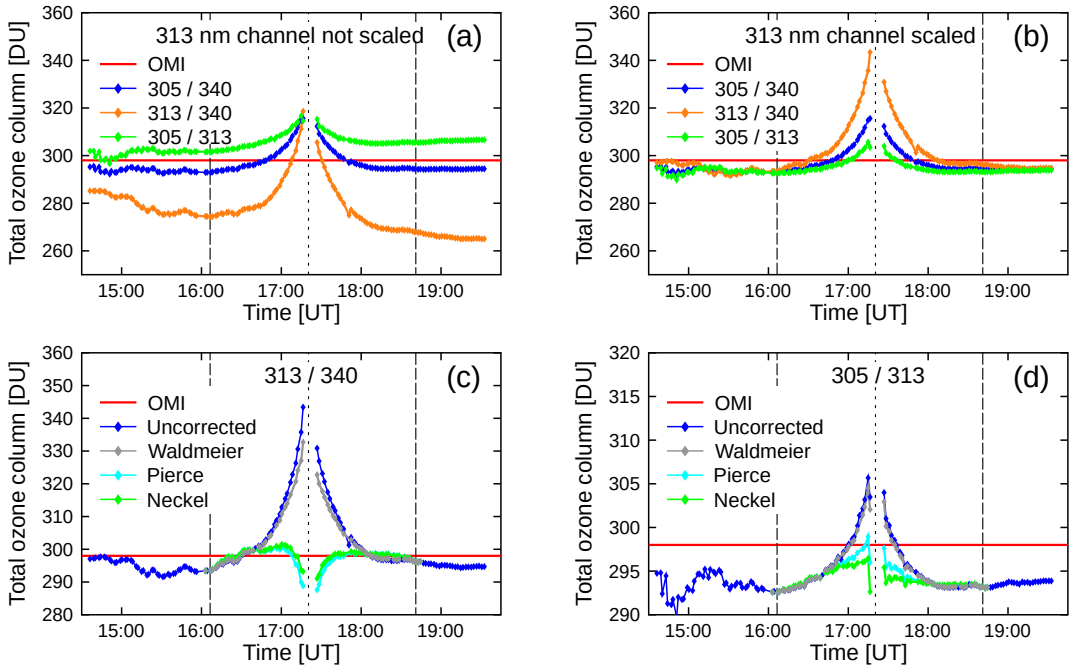

Fig. S3. Total ozone column derived from global irradiance measurements of the GUVis-3511 radiometer using different wavelength pairs. Panel (a): comparison of ozone retrievals with the 305 / 340 pair (blue), the 313 / 340 pair (orange), and the 305 / 313 pair (green). Panel (b): same as Panel (a) but measurements of the 313 nm channel were scaled with a factor of 0.95 before calculating TOC. Panel (c): TOC retrievals for the 313 / 340 pair using either no correction (blue), or the LD-corrections by Waldmeier (grey), Pierce (cyan), and Neckel (green). Panel (d): same as Panel (c) but for the 305 / 313 pair. Measurements of the 313 nm channel were scaled by 0.95 for retrievals shown in Panels (c) and (d). Long-dashed lines indicate the start and end times of the eclipse and the short-dashed line indicates the time at totality. Note that y-scales of the various panels differ.

TOC data shown in Figs. S3c and S3d were corrected for the LD-effect similar to the TOC data derived from the 305 / 340 pair shown in Fig. 7. As in that figure, TOCs calculated for the 313 / 340 and 305 / 313 pairs (Fig. S3c and S3d, respectively) spike at the time of totality when no LD correction is applied. The LD correction by Waldmeier has only a marginal effect on this result. In contrast, LD corrections using either the parameterizations by Pierce or Neckel greatly decrease this spurious spike. For example without LD correction, the TOC calculated with the 313 / 340 pair is 50 DU higher shortly before totality compared to the TOC at 1st contact. Using the LD correction by Neckel, TOC remains constant to within ±5.3 DU or ±1.8 %. Similarly, the TOC calculated with the 305 / 313 pair is 13 DU higher shortly before totality compared to the TOC at 1st contact while TOC remains constant to within ±2.0 DU or ±0.7 %.

Calculations of TOCs from global irradiance using the 305 / 313 and 313 / 340 wavelength pairs confirm the conclusions reached from results of the 305 / 340 nm pair. Specifically, we did not find evidence that bow waves from the Moon's shadow lead to oscillations in TOC as observed by Zerefos (2000; 2007) and Mims and Mims (1993) during previous solar eclipses.

References

Anderson, G. P., Clough, S. A., Kneizys, F. X., Chetwynd, J. H., and Shettle, E. P.: AFGL atmospheric constituents profiles (0 – 120 km), Tech. Rep. AFGL-TR-86-0110, Air Force Geophys. Lab., Hanscom Air Force Base, Mass., 1986.

Bass, A. and Paur R. J.: The ultraviolet cross sections of ozone: 1, The measurement, in Atmospheric Ozone, edited by C. Zerefos and A. Ghazi, pp. 606–616, D. Reidel, Norwell, Mass., 1985.

Bernhard, G. and Seckmeyer, G.: Uncertainty of measurements of spectral solar UV irradiance. J. Geophys. Res., 104(D12), 14321–14345, https://doi.org/10.1029/1999JD900180, 1999.

Bernhard, G., Booth, C. R., and Ehramjian, J. C.: Version 2 data of the National Science Foundation's Ultraviolet Radiation Monitoring Network – South Pole, J. Geophys. Res., 109, D21207, doi:10.1029/2004JD004937, 2004.

Booth, C. R., Lucas, T. B., Morrow, J. H., Weiler, C. S., and Penhale, P. A.: The United States National Science Foundation's polar network for monitoring ultraviolet radiation, in Ultraviolet Radiation in Antarctica: Measurements and Biological Effects, Antarc. Res. Ser., vol. 62, edited by C. S. Weiler and P. A. Penhale, pp. 17–37, AGU, Washington, D. C., https://doi.org/10.1029/AR062p0017, 1994.

Gueymard, C. A.: The sun's total and spectral irradiance for solar energy applications and solar radiation models, Solar Energy, 76(4), 423–453, https://doi.org/10.1016/j.solener.2003.08.039, 2004.

Mayer, B. and Kylling, A.: The libRadtran software package for radiative transfer calculations-description and examples of use, Atmos. Chem. Phys., 5(7), 1855–1877, https://doi.org/10.5194/acp-5-1855-2005, 2005.

Mims III, F. M. and Mims, E. R.: Fluctuations in column ozone during the total solar eclipse of July 11, 1991, Geophys. Res. Lett., 20(5), 367–370, https://doi.org/10.1029/93GL00493, 1993.

Ricchiazzi, P., Yang, S., Gautier, C., and Sowle, D.: SBDART: A research and teaching software tool for plane-parallel radiative transfer in the Earth's atmosphere, B. Am. Meteorol. Soc., 79(10), 2101–2114, https://doi.org/10.1175/1520-0477(1998)079<2101:SARATS>2.0.CO;2, 1998.

Seckmeyer, G., Bais, A., Bernhard, G., Blumthaler, M., Johnsen, B., Lantz, K., and McKenzie, R.: Instruments to measure solar ultraviolet radiation, Part 3: Multi-channel filter instruments. World Meteorological Organization Global Atmosphere Watch, Report 190, WMO TD 1537, 51 pp., 2010.

Yoon, H. W., Gibson, C. E., and Barnes P. Y.: Realization of the National Institute of Standards and Technology detector-based spectral irradiance scale, Appl. Opt., 41(28), 5879–5890, https://doi.org/10.1364/AO.41.005879, 2002.

Zerefos, C. S., Balis, D. S., Meleti, C., Bais, A. F., Tourpali, K., Kourtidis, K., K. Vanicek, K., Cappellani, F., Kaminski, U., Colombo, T., and Stübi, R.: Changes in surface solar UV irradiances and total ozone during the solar eclipse of August 11, 1999, J. Geophys. Res., 105(D21), 26463–26473, https://doi.org/10.1029/2000JD900412, 2000.

Zerefos C. S., Gerasopoulos E., Tsagouri I., Psiloglou B. E., Belehaki A., Herekakis T., Bais A., Kazadzis S., Eleftheratos C., Kalivitis N., and Mihalopoulos N.: Evidence of gravity waves into the atmosphere during the March 2006 total solar eclipse, Atmos. Chem. Phys., 7(18), 4943–4951, https://doi.org/10.5194/acp-7-4943-2007, 2007.